Nonlinear behavior of deep reinforced concrete coupling beams

Z.Z. Zhao†

Department of Civil Engineering, Tsinghua University, Beijing, China

A.K.H. Kwan‡

Department of Civil Engineering, The University of Hong Kong, Hong Kong SAR, China

Abstract. Six large scale models of conventionally reinforced concrete coupling beams with span/depth ratios ranging from 1.17 to 2.00 were tested under monotonically applied shear loads to study their nonlinear behavior using a newly developed test method that maintained equal rotations at the two ends of the coupling beam specimen and allowed for local deformations at the beam-wall joints. By conducting the tests under displacement control, the post-peak behavior and complete load-deflection curves of the coupling beams were obtained for investigation. It was found that after the appearance of flexural and shear cracks, a deep coupling beam would gradually transform itself from an ordinary beam to a truss composed of diagonal concrete struts and longitudinal and transverse steel reinforcement bars. Moreover, in a deep coupling beam, the local deformations at the beam-wall joints could contribute significantly (up to the order of 50%) to the total deflection of the coupling beam, especially at the post-peak stage. Finally, although a coupling beam failing in shear would have a relatively low ductility ratio of only 5 or even lower, a coupling beam failing in flexure could have a relatively high ductility ratio of 10 or higher.

Key words: reinforced concrete; coupling beams; shear walls.

1. Introduction

It is well known that in a reinforced concrete coupled shear wall structure, both the strength and ductility of the coupling beams have great influence on the aseismic performance of the structural system (Paulay 1970). Since coupling beams are generally formed between door or window openings, which are usually less than 2.0 m wide, most of them are relatively short and deep. For deep coupling beams, i.e., coupling beams with small span/depth ratios, providing appropriate strength presents no particular difficulties. However, since they tend to fail in shear, providing sufficient ductility can be quite difficult. Moreover, it had been found that deep coupling beams with span/depth ratios smaller than 2.0 behave quite differently from the ordinary beams in frame structures (Paualy 1971, Tassios *et al.* 1996, Kwan and Zhao 1998). Although at the elastic stage,

† Lecturer
‡ Professor

such a deep coupling beam behaves like an ordinary beam, after the appearance of cracks, the coupling beam behaves more like a truss composed of diagonal concrete struts and longitudinal and transverse reinforcement bars. The transverse component of the compression forces developed in the diagonal struts resists the applied shear load whereas the longitudinal component pushes the walls at the two ends apart causing the beam to elongate and the longitudinal reinforcement bars to be in tension.

One major difficulty in the design of deep reinforced concrete coupling beams is the prevention of shear failure (Paulay 1971, Barney *et al.* 1980). In general, a deep coupling beam would tend to fail in a shear-tension mode, in which the coupling beam is split into two triangular halves tied together by the transverse reinforcement and failure is caused by yielding of the transverse reinforcement. This failure mode can be avoided by increasing the transverse reinforcement. However, with increased transverse reinforcement, the coupling beam would tend to fail in a shear-compression mode, which is caused by crushing of the concrete at where the diagonal struts act against the walls. Furthermore, under cyclic loading, a deep coupling beam might also fail in a shear-sliding mode. In this failure mode, the coupling beam slides along transverse cracks at the beam-wall joints, which are formed by bending cracks cutting through the whole beam section due to load reversal. It seems that the best way of avoiding shear failure is to limit the flexural capacity of the coupling beam so that the beam would fail only in flexure, not in shear.

Another difficulty in the design of deep coupling beams is an accurate prediction of the nonlinear load-deflection behavior, which is needed for ductility evaluation and push-over analysis of the coupled shear wall structure. In previous experimental studies, the measured deflections were often considerably in excess of the theoretically predicted values (Lybas 1981, Aristizabal-Ochoa 1982, Aktan and Bertero 1984). This had been attributed partly to the local deformation of the walls near the beam-wall joints, partly to the bond-slip of the longitudinal reinforcement bars at the beam-wall joints, and partly to the presence of pre-existing cracks at the beam-wall joints. Although the possible influences of the local joint deformations are by now quite well recognized, there have been very few studies on the details of the local deformations at the beam-wall joints or on quantitative analysis of their effects. Without the local joint deformations fully allowed for, any evaluation of the nonlinear load-deflection curves or ductility of deep coupling beams would be incomplete.

Most previous tests on coupling beams were conducted by applying equal contraflexural moments to the two ends of the coupling beam specimen (Paulay 1971, Tassios *et al.* 1996, Paulay and Binney 1974). With the loads applied in this way, the boundary conditions of a real coupling beam could be very well simulated before the beam specimen started to crack. However, after the beam specimen had cracked, since there might be more cracks at one end than the other, the rotations at the two ends of the coupling beam specimen could be quite different, as had been observed by some investigators (Paulay and Binney 1974). This had violated the condition in a coupled shear wall structure that the two walls at the ends of a coupling beam should remain parallel or rotate by the same amount. To properly simulate the boundary conditions of a real coupling beam, the rotations at the two ends of the beam specimen must be controlled to be equal.

To resolve the afore-mentioned problems with the existing test methods, the authors have recently developed a new method of testing coupling beams, in which the rotations at the two ends of the beam specimen are controlled to be equal and the local deformations at the beam-wall joints are fully allowed for (Kwan and Zhao 1999). Trial testing has verified that the newly developed method is particularly suitable for studying the post-peak behavior and measuring the ductility of deep

reinforced concrete coupling beams. In the study reported herein, this method was employed to test conventionally reinforced concrete coupling beams with span/depth ratios varying from 1.17 to 2.00. The purpose was to investigate the nonlinear behavior of deep conventionally reinforced concrete coupling beams, which are known to behave quite differently from the ordinary beams in frame structures. The results should be useful for evaluating the strength and ductility of deep coupling beams, development of a nonlinear structural model for coupling beams, and push-over analysis of coupled shear wall structures.

2. Experimental program

2.1 Specimen design

Six conventionally reinforced concrete coupling beams were fabricated for testing. Details of the beam specimens are shown in Fig. 1, while the structural parameters of the beam specimens are listed in Table 1. The beam specimens were basically 1/2-scale models of typical coupling beams in real structures. Each coupling beam specimen comprised of three parts: a central portion
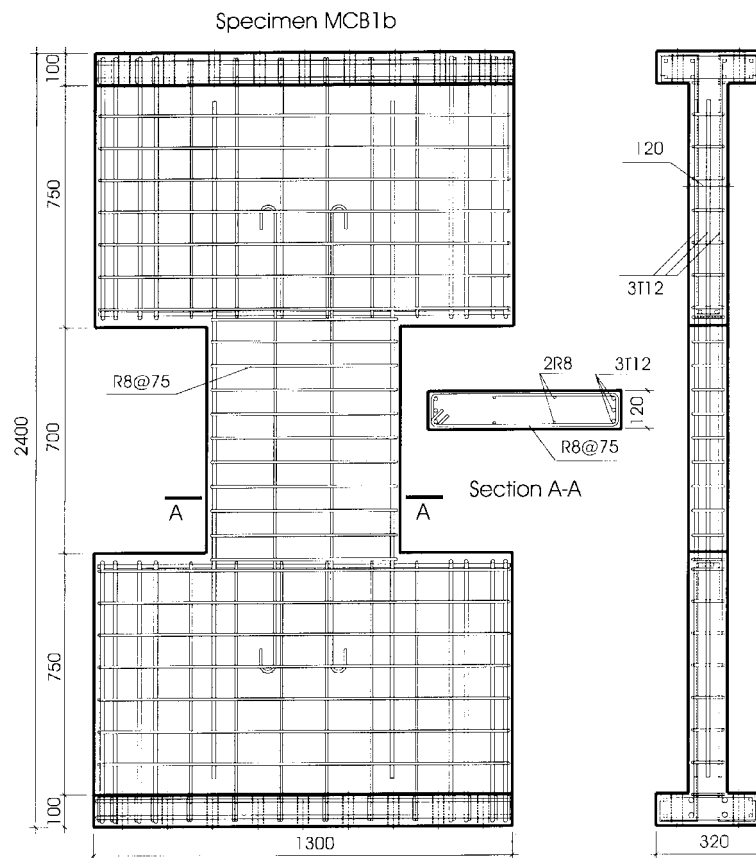

Fig. 1 Details of beam specimens tested

Table 1 Structural parameters of the beam specimens tested

Model no.	Span/depth ratio	Top or bottom longitudinal reinforcement (ratio)	Additional longitudinal reinforcement	Transverse reinforcement (ratio)
MCB1a	1.17	3T12 (0.49%)	4R8	R8 @ 72c/c (1.11%)
MCB1b	1.17	3T12 (0.49%)	4R8	R8 @ 75c/c (1.07%)
MCB2a	1.40	3T12 (0.59%)	4R8	R8 @ 80c/c (1.00%)
MCB2b	1.40	2T12 + T8 (0.49%)	4R8	R8 @ 75c/c (1.07%)
MCB3	1.75	2T12 (0.50%)	2R8	R8 @ 75c/c (1.07%)
MCB4	2.00	T12+2T8 (0.56%)	2R8	R8 @ 75c/c (1.07%)

Note: (1) T denotes high-yield deformed bars and R denotes mild steel plain round bars.
         (2) @ × c/c means at a center-to-center spacing of *x* mm.

representing the coupling beam itself and two end blocks representing parts of the walls connected to the ends of the coupling beam. The thickness and clear span of the beam portion were fixed at 120 mm and 700 mm respectively, whereas the depth of the beam portion was varied to give four different span/depth ratios. The end blocks were rectangular in shape having the same thickness as the beam. They were each of size 1300 mm × 750 mm, which should be large enough to accommodate all the local deformations near the beam-wall joints. At the far end edge of each end block, a flange 320 mm wide by 100 mm thick was provided for connecting the specimen to the testing frame.

In the beam portion of each specimen, longitudinal and transverse reinforcement were provided. The longitudinal reinforcement consisted of main reinforcement placed at the top and bottom of the beam section and additional reinforcement placed near mid-depth of the beam section. All the longitudinal reinforcement bars in the beam were provided with generous anchorage into the end blocks. On the other hand, the transverse reinforcement was provided in the form of single stirrups equally spaced within the span of the beam. Inside each of the two end blocks, nominal reinforcement was provided to avoid premature failure of the end blocks.

The specimens MCB1a and MCB1b have the same span/depth ratio of 1.17 and the same longitudinal reinforcement but slightly different transverse reinforcement. MCB1a was the first specimen fabricated for testing. However, during testing, it failed prematurely after the main reinforcement had yielded due to breakage of one of the flanges connecting the specimen to the testing frame. Subsequently, all the other specimens were provided with heavier reinforcement in the flanges and such kind of failure never happened again. The specimens MCB2a and MCB2b have the same span/depth ratio of 1.40 but different longitudinal and transverse reinforcement. Lastly, the specimens MCB3 and MCB4 have span/depth ratios of 1.75 and 2.00 respectively. They have approximately the same main reinforcement ratios as those of MCB1b and MCB2b. By keeping the main reinforcement ratios of the beam specimens practically constant, the specimens with smaller span/depth ratios would have higher flexural to shear strength ratios and would thus tend to fail in shear, while the specimens with larger span/depth ratios would have lower flexural to shear strength ratios and would thus tend to fail in flexural.

2.2 Materials and construction

The concrete used was made from ordinary Portland cement and crushed granitic aggregate having a maximum size of 10 mm. All beam specimens were cast with their planes lying

horizontally. They were moist cured for 7 days and thereafter stored under ambient condition. Along with each beam specimen, three 150 mm × 300 mm cylinders and three 150 mm cubes were cast, cured side by side with the beam specimen and tested at the same time when the beam specimen was tested. The beam specimens and the concrete cylinders and cubes were generally tested at ages of 33 to 52 days. At the time of testing, the average cylinder and cube strengths of the concrete were 41.0 and 53.4 MPa respectively.

High-yield deformed bars were used for the main longitudinal reinforcement placed at the top and bottom of the beam sections, whereas mild steel plain round bars were used for the additional longitudinal reinforcement placed at mid-depth of the beam sections and the transverse reinforcement. The high-yield bars were of two sizes. Those with 12 mm diameter had yield and ultimate strengths of 525 and 636 MPa and a plastic elongation strain of 18%, while those with 8 mm diameter had yield and ultimate strengths of 517 and 717 MPa and a plastic elongation strain of 17%. On the other hand, the mild steel bars were all of size 8 mm and had yield and ultimate strengths of 336 and 440 MPa and a plastic elongation strain of 25%.

2.3 Test set-up and loading program

Fig. 2 shows the arrangement of the test set-up. As shown in the figure, the beam specimen was erected with the longitudinal axis of the beam in the vertical direction. It was fixed at one end to a rigid ground beam and connected at the other end to a T-shaped steel loading frame. Lateral load was applied to the specimen through the loading frame by a servo-controlled hydraulic actuator, whose loading and support ends were pin-connected to the loading frame and a horizontal reaction frame respectively. The line of action of the applied load was aligned to pass through the center of the beam specimen. A rotation restraining mechanism consisting of two parallelogram-shaped pin-jointed trusses was installed to ensure that the rotations of the two ends of the specimen were equal. The two parallelogram-shaped trusses were designed to be totally free to have their shapes deformed but the opposite edges of each parallelogram would always remain parallel. Thus, the two parallelogram-shaped trusses would not impose any restraint against the longitudinal or transverse movement of the specimen but would restrain the two ends of the specimen to remain parallel. Out-
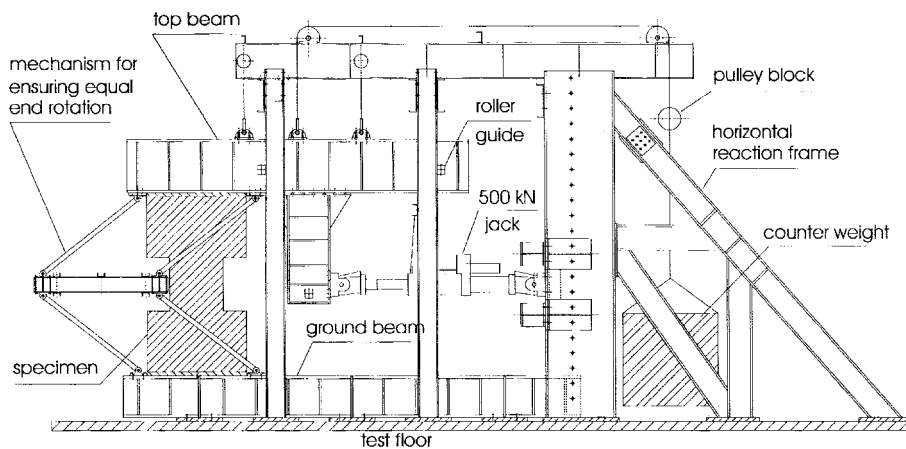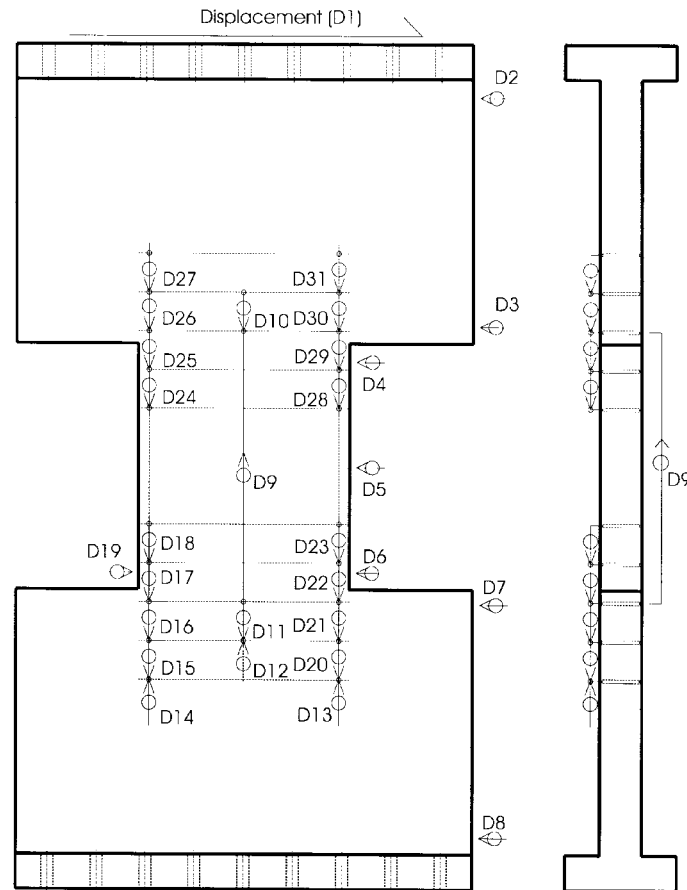

Fig. 2 Test set-up

Fig. 3 Layout of the LVDTs

of-plane movements of the loading frame were restrained by the provision of roller guides. Self-weight of the loading frame was balanced by a counter weight through a pulley system.

On each coupling beam specimen, more than 30 LVDTs were mounted, as shown in Fig. 3. Some LVDTs were installed on an isolated frame to measure the absolute deflection of the specimen while others were mounted on the specimen to measure the deformations of the beam itself and the joints. At the same time, in each coupling specimen, about 50 electrical resistance strain gauges were glued on selected longitudinal and transverse reinforcement bars to measure the strains developed in the reinforcement bars. All signals from the LVDTs and the strain gauges were digitized and recorded by a computer controlled data acquisition system.

The load was applied monotonically to the coupling beam specimen basically under displacement control. At the beginning of the tests, however, in order to study in details the load levels at which the various cracks appeared and the reinforcement started to yield, the load was applied under load control in steps of 10 or 20 kN. After the maximum strain in the main reinforcement had approached the yield strain, the load was applied under displacement control in steps of 0.5 to 1.0 mm until the specimen failed. As far as possible, each test was carried out until the load resisting capacity of the beam had, after reaching the peak, dropped to less than 85% of the peak load.

3. Experimental results

3.1 General behavior and failure modes

The crack patterns of the six beam specimens after completion of the tests are depicted in Fig. 4. At the beginning, all beam specimens had similar crack patterns. Flexural cracks were first observed at the tension corners of the beam-wall joints. As the applied load increased, these flexural cracks extended into the wall panels and then turned to run parallel to the beam-wall interfaces. At the same time, new flexural cracks appeared inside the beams at their tension sides. Upon further loading, many of these flexural cracks turned to an inclined direction and propagated towards the compression corners at the beam-wall joints to become combined flexural and shear cracks. Meanwhile, numerous fine cracks also appeared in the wall panels. However, after the main

(a) MCB1a (upper flange failure)   (b) MCB1b (shear-tension failure)   (c) MCB2a (shear-tension failure)

(d) MCB2b (flexural failure)   (e) MCB3 (flexural failure)   (f) MCB4 (flexural failure)
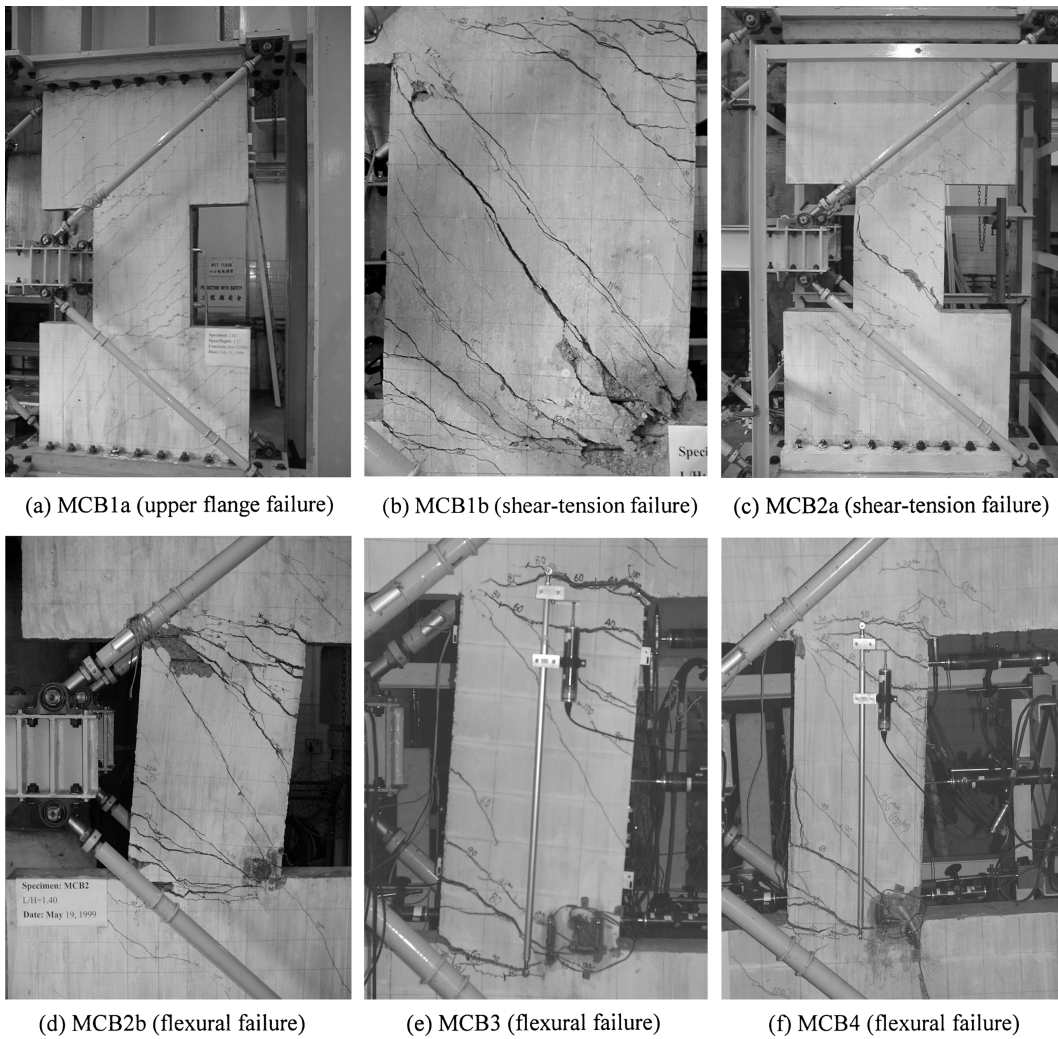
Fig. 4 Crack patterns and failure modes of the beam specimens

reinforcement had yielded, the crack patterns of the specimens became different.

In each of the specimens MCB1a and MCB1b, which had very small span/depth ratios, an inclined shear crack appeared at the center of the beam right after the main reinforcement had yielded. The shear crack gradually developed and divided the beam into two triangular halves interconnected by the transverse reinforcement. As the deflection of the specimen further increased, the flexural cracks near the beam-wall joints gradually opened up while the inclined shear crack remained stable. At this stage, MCB1a failed due to breakage of one of its flanges and the test had to be terminated before the ultimate state was reached. On the other hand, the specimen MCB1b, whose flanges were more heavily reinforced, did not have such problem. As the test of MCB1b continued, shortly after the main reinforcement had yielded, the transverse reinforcement also started to yield. Upon reaching the peak load, nearly all transverse reinforcement bars had yielded and the inclined shear crack opened up quickly. Eventually when the width of the shear crack reached about 10 mm, the concrete at the compression corners of the beam was crushed and the beam specimen failed in a shear-tension mode.

Although the specimens MCB2a and MCB2b had the same span/depth ratio, they behaved quite differently because of the difference in reinforcement details. In specimen MCB2a, an inclined shear crack appeared at the center of the beam even before the main reinforcement started to yield. It remained a very fine crack until the main reinforcement yielded. As the main reinforcement yielded, the transverse reinforcement also started to yield and soon afterwards the shear crack developed rapidly and the specimen failed in a shear-tension mode. In specimen MCB2b, the inclined shear crack appeared after the main reinforcement had yielded when the deflection of the beam was almost two times the deflection at yield (the deflection when the main reinforcement started to yield). This crack gradually developed in length and width but never became critical. On the other hand, the flexural cracks at the beam-wall joints and the combined flexural and shear cracks at the tension sides of the beam continued to develop as the deflection of the beam increased. Finally, the concrete at the compression zones was crushed, one main reinforcement bar was broken and the beam failed in flexure.

In each of the specimens MCB3 and MCB4, which had approximately the same longitudinal and transverse reinforcement ratios as those of the specimens MCB1b and MCB2b but larger span/depth ratios, inclined shear cracks were also formed at the center of the beam after the main reinforcement had yielded. However, these shear cracks were generally formed at much later times when the deflections of the beams were already very large and they did not develop even when the beam specimens failed. After entering into the post-peak stage, the flexural cracks at the beam-wall joints opened up quickly and eventually both MCB3 and MCB4 failed in flexure with noticeable rotations at the beam-wall joints. In the case of MCB3, one main reinforcement bar was broken before the load resisting capacity of the beam specimen had dropped to less than 85% of the peak load and the test was stopped.

3.2 Load-deflection characteristics

The load-deflection curves of the six beam specimens are plotted in Fig. 5. It should be noted that the deflections used for plotting these curves were the relative lateral displacements of the beam specimens measured along the far end edges of the end blocks at the ends of the beams and thus they included the deflections of the beams and the deflections due to local deformations at the beam-wall joints.

(a) MCB1a and MCB1b (span/depth=1.17)

(b) MCB2a and MCB2b (span/depth=1.40)

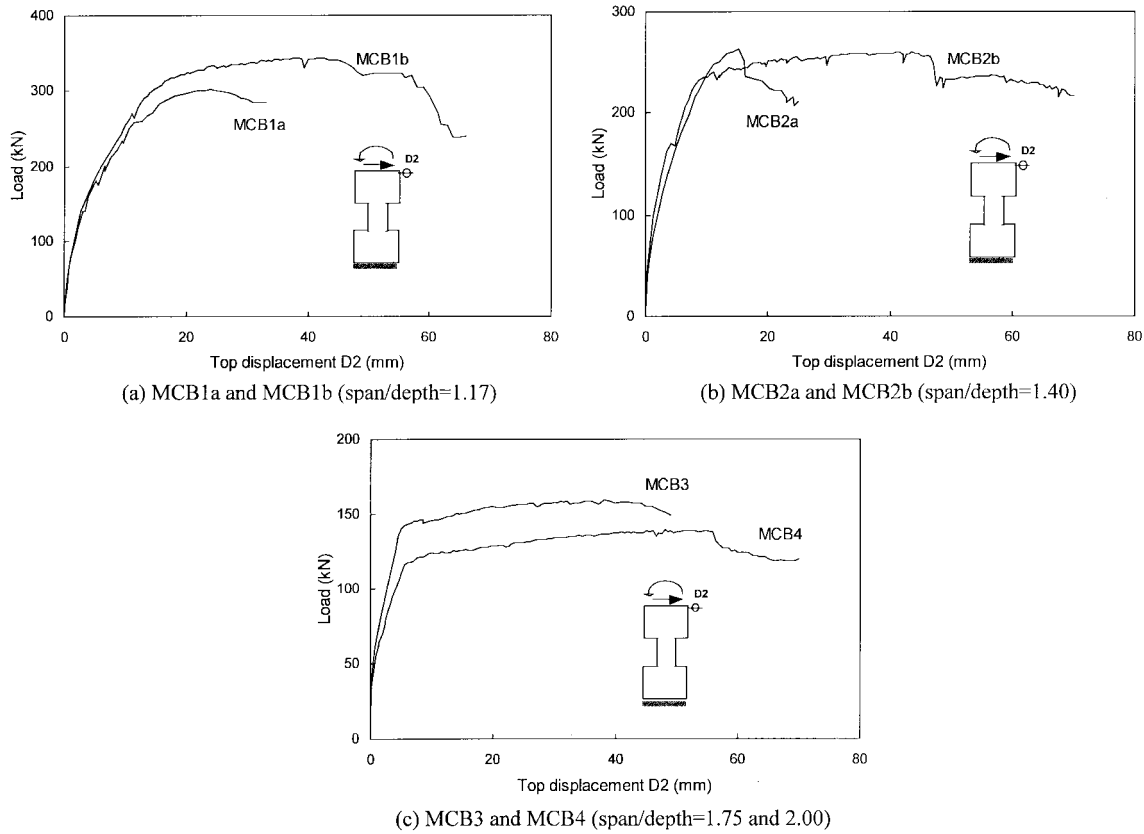
(c) MCB3 and MCB4 (span/depth=1.75 and 2.00)

Fig. 5 Load-deflection curves of the beam specimens

From the load-deflection curves of MCB1a and MCB1b, which were almost identical except for a small difference in the transverse reinforcement, it is evident that the ascending branches of the two curves agreed with each other closely. However, due to premature failure of MCB1a, the descending branch of its load-deflection curve was not obtained and therefore no comparison between the descending branches of the two curves could be made. Nevertheless, it can be seen that the load-deflection curve of MCB1b, which failed in shear, had no obvious yield point but a fairly long post-peak range up to a deflection of about 60 mm. The ascending branches of the load-deflection curves of MCB2a and MCB2b also agreed with each other closely but since the two specimens failed in different modes, the descending branches of their load-deflection curves were distinctly different. Relatively, the descending branch of MCB2a was very short and sharp, revealing that MCB2a failed in a brittle manner. On the other hand, the load-deflection curve of MCB2b contained a clearly defined yield point and fairly long yielding and post-peak ranges up to a deflection of about 70 mm, indicating a ductile failure mode. Like that of MCB2b, the load-deflection curves of MCB3 and MCB4, which failed in flexure, had obvious yield points and fairly long yielding and post-peak ranges up to deflections of about 50 mm and 70 mm respectively.

From the above, it can be seen that apart from MCB1a and MCB2a, all the specimens MCB1b, MCB2b, MCB3 and MCB4 were capable of sustaining a maximum lateral deflection of about 50 mm before their load resisting capacities dropped significantly. Since the beam specimens had a

Table 2 Summary of test results

Model no.	Failure mode	Load (kN)		Deflection (mm)			Ductility ratio (D_u/D_y)
		at yield V_y	at peak V_p	at yield D_y	at peak D_p	at ultimate D_u	
MCB1a	premature	258	301	11.50	-	-	-
MCB1b	shear-tension	262	344	10.50	42.50	60.00	5.7
MCB2a	shear-tension	228	262	9.08	15.40	22.00	2.4
MCB2b	flexure	198	260	5.97	41.04	69.00	11.6
MCB3	flexure	126	159	4.00	38.00	49.00	12.3
MCB4	flexure	100	140	4.16	48.20	70.00	16.8

clear span of 700 mm, such a maximum deflection capacity of 50 mm represented a maximum drift ratio (lateral deflection per clear span ratio) of 7%, a good value judging from the relatively small span/depth ratios of the beam specimens.

3.3 Strength and ductility

A summary of the strength and ductility of each beam specimen is presented in Table 2. In this table, the load at yield was the load when the main reinforcement started to yield and the load at peak was the maximum applied load during the test. On the other hand, the ductility was evaluated in terms of a ductility ratio defined as the ratio of the deflection at ultimate to the deflection at yield. The deflection at ultimate was taken as the deflection at the post-peak stage when the load resisting capacity dropped to 85% of the peak load, whereas the deflection at yield was taken as the deflection when the main reinforcement started to yield.

Up to the point when the main reinforcement started to yield, MCB1a and MCB1b behaved quite similarly and therefore they had similar yield load and similar deflection at yield. However, since MCB1a failed prematurely due to breakage of one of its flanges, the peak load given in Table 2 was only the maximum load applied during the test; the specimen might be able to reach a higher peak load if it did not fail prematurely. For this reason, the ductility ratio of MCB1a was not evaluated. Nevertheless, the ductility ratio of MCB1b had been evaluated as 5.7, which was not too bad for a shear mode of failure.

Comparing between the two specimens MCB2a and MCB2b, which had the same span/depth ratio, MCB2a had about 15% higher yield load. This was because MCB2a was provided with a larger amount of main reinforcement. Although MCB2a should have a higher flexural strength, since it finally failed in shear, its strength was actually governed by the transverse reinforcement and was only marginally higher than that of MCB2b. Moreover, due to shear failure, MCB2a had a very low ductility ratio of only 2.4. On the other hand, the specimen MCB2b, which failed in flexure, had achieved a much higher ductility ratio of 11.6.

Regarding the last two specimens MCB3 and MCB4, although they had lower strength than the other specimens, they had relatively high ductility ratios of 12.3 and 16.8 respectively because they both failed in flexure. In the case of MCB3, since the test was stopped due to breakage of one main reinforcing bar before the load resisting capacity dropped to less than 85% of the peak load, the deflection at ultimate was taken as the deflection when the main bar was broken for evaluating the ductility ratio.

Table 3 Experimental results and corresponding theoretically predicted values

Model no.	Experimental strength (kN)		Theoretical flexural strengths (kN)		Theoretical shear strength (kN)		
	V_y	V_p	V_{y1}	V_{y2}	V_c	V_s	V
MCB1a	258	301	276	329	74	266	340
MCB1b	262	344	276	329	77	255	332
MCB2a	228	262	226	269	61	198	258
MCB2b	198	260	187	229	64	211	275
MCB3	126	159	117	134	44	166	211
MCB4	100	140	98	112	40	144	184

It should, however, be noted when interpreting the above results that these ductility ratios were obtained under monotonic loading. Under cyclic loading, a coupling beam could degrade fairly rapidly and the actual ability of the coupling beam to withstand reversed inelastic deformation might not be as good as might be inferred from these relatively high ductility ratios. Separate cyclic loading tests are needed to evaluate the cyclic load performance of the coupling beams.

The coupling beam specimens have been analyzed for their theoretical strengths using the method given in ACI 318-95 (Paulay and Binney 1974). Since a coupling beam could fail in flexure or in shear, it was necessary to evaluate both the flexural strength (strength based on flexural failure) and the shear strength (strength based on shear failure) of the beam. The smaller of the flexural strength and the shear strength would be the predicted strength. Table 3 presents the comparison of the flexural and shear strengths evaluated by ACI 318-95 with the measured strengths.

For each coupling beam analyzed, two flexural strength values, V_{y1} and V_{y2}, were obtained. V_{y1} was evaluated with the contribution of the additional reinforcement ignored while V_{y2} was evaluated with the contribution of the additional reinforcement taken into account. It is seen that in all the cases studied, V_{y2} was greater than V_{y1} by at least 15%. Comparing V_{y1} and V_{y2} to the measured yield load V_y, it is evident that in all cases, including those involving shear failure, the values of V_y agreed quite closely with the corresponding values of V_{y1}. Comparing V_{y1} and V_{y2} to the measured peak load V_p for coupling beams failing in flexure, it can be seen that the values of V_p generally agreed more closely with the values of V_{y2} than with the values of V_{y1}. Hence, for estimation of flexural strength, V_{y2} should be used instead of V_{y1}. Moreover, the V_p values of the coupling beams failing in flexure were generally higher than the V_{y2} values evaluated using the yield strengths of the reinforcement bars. Strain hardening of the longitudinal reinforcement might have contributed significantly to the flexural strengths of the coupling beam specimens tested.

According to ACI 318-95, the shear strength V is equal to the sum of the shear capacity of the concrete V_c and the shear capacity of the stirrups V_s. Theoretically, if V is smaller than V_{y2}, the coupling beam should fail in shear and if V is larger than V_{y2}, the coupling beam should fail in flexure. However, if V and V_{y2} are close to each other, then either failure mode may occur. For instance, in the case of MCB1b, although the estimated value of V (332 kN) was larger than the estimated value of V_{y2} (329 kN), the beam specimen actually failed in shear. It was quite possible that strain hardening of the main reinforcement had increased the true value of V_{y2} to larger than the value of V. In all other cases, where V is at least 20% larger than V_{y2}, the beam specimens failed in flexure.

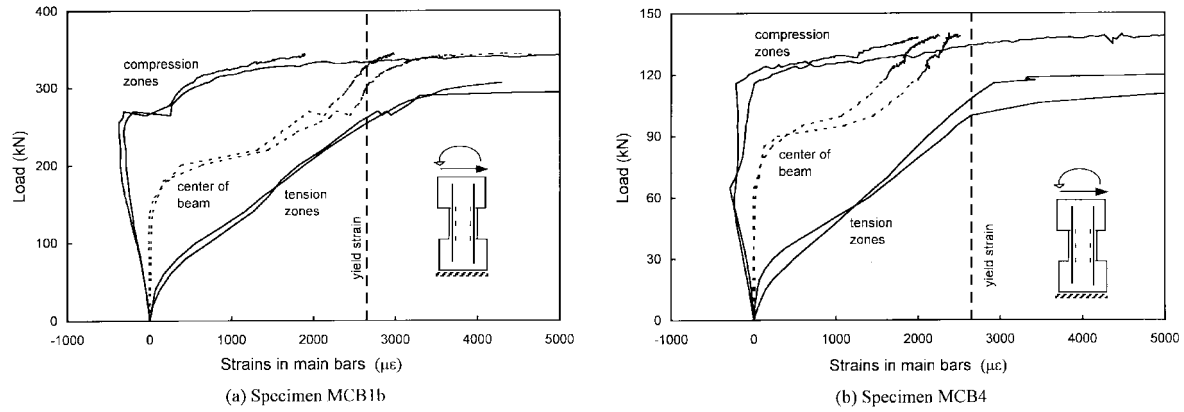(a) Specimen MCB1b   (b) Specimen MCB4

Fig. 6 Strain distribution in main reinforcement of specimens MCB1b and MCB4

3.4 Strain distributions in reinforcement bars

Fig. 6 shows the variation of the axial strains in the longitudinal reinforcement bars with the applied shear load for the beam specimens MCB1b and MCB4, which had span/depth ratios of 1.17 and 2.00 respectively. The other beam specimens had similar axial strains developed in their longitudinal reinforcement bars and thus for brevity their results are not presented. It is seen that in each of the specimens MCB1b and MCB4, at small applied load before cracks appeared in the beam, the axial strains developed in the longitudinal reinforcement bars corresponded to a contraflexural moment distribution along the length of the beam. The contraflexural moments acting on the beam resulted in equal end moments at the ends and zero moment at the center of the beam. The end moments caused the longitudinal reinforcement bars near the ends of the beam to be subjected to tension on one side and compression on the other side, while the zero moment at the center caused the longitudinal reinforcement bars at the center of the beam to remain unstressed, as in an ordinary beam. Hence, before cracks appeared, the coupling beams behaved like ordinary beams.

After the appearance of flexural and shear cracks, however, the strain distribution in the longitudinal reinforcement bars of the coupling beam started to change. Firstly, the rate of increase of the tensile strain in the longitudinal reinforcement with the applied load gradually increased while the rate of increase of the compressive strain in the longitudinal reinforcement with the applied load gradually decreased. As a result, the tensile strain developed in the longitudinal reinforcement near the ends of the beam became significantly larger than the corresponding compressive strain developed in the longitudinal reinforcement at the same end but opposite side of the beam. Secondly, at a certain stage, the compressive strain in the longitudinal reinforcement near the ends of the beam stopped increasing and then started to decrease causing the strain to eventually become tensile. Thirdly, significant tensile strains were developed in all the longitudinal reinforcement bars at the center of the beam despite zero moment acting there. Finally, all the longitudinal reinforcement bars were in tension throughout the entire length of the beam. All these changes indicated that after the appearance of flexural and shear cracks, the coupling beams started to elongate and no longer behaved like ordinary beams.

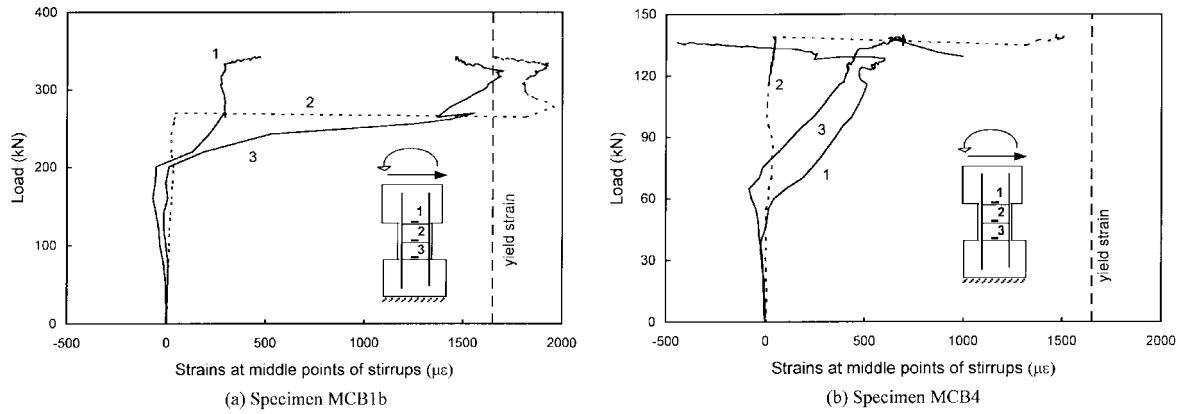Fig. 7 presents the measured axial strains in the transverse reinforcement bars (stirrups) of

(a) Specimen MCB1b

(b) Specimen MCB4

Fig. 7 Strain distribution in stirrups of specimens MCB1b and MCB4

(a) Load-elongation strain of the beam specimens

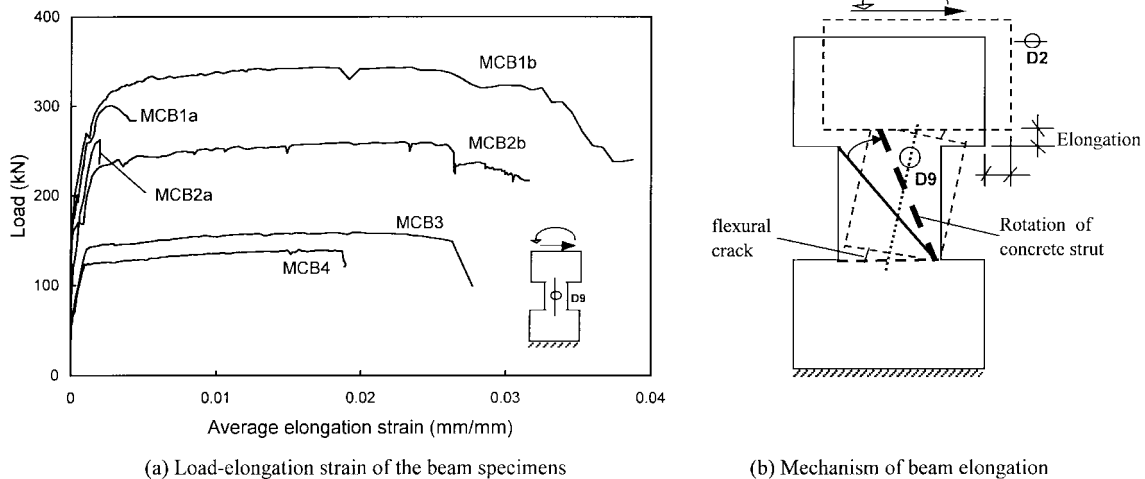(b) Mechanism of beam elongation

Fig. 8 Axial elongations of the beam specimens tested

specimens MCB1b and MCB4. In specimen MCB1b, before the appearance of inclined shear cracks, the axial strains in the stirrups remained very small. However, after the appearance of inclined shear cracks, the axial strains in the stirrups increased rapidly and after slight further increase in applied load, some stirrups already started to yield. Eventually, when peak load was reached, nearly all the stirrups yielded leading to shear failure of the beam specimen. In specimen MCB4, the axial strains in the stirrups increased slowly up to at most one-third of the yield strain even when inclined shear cracks appeared. Thereafter, the axial strains in the stirrups continued to increase but remained smaller than the yield strain throughout the test indicating that the stirrups in MCB4 had successfully restrained the development of the inclined shear cracks and prevented shear failure of the specimen.

3.5 Axial elongation

Fig. 8(a) depicts the variation of the axial elongation of each coupling beam specimen during the

test by plotting the applied shear load against the corresponding axial elongation. The axial elongation was measured by a LVDT mounted along the longitudinal axis of the beam specimen with each of its two ends attached to one end block and the results were expressed in terms of an average axial elongation strain (amount of axial elongation divided by gauge length). It can be seen from the curves plotted that the specimen MCB1a, which failed prematurely, and the specimen MCB2a, which failed in a very brittle manner, both exhibited little axial elongation even when they failed completely. However, the other specimens MCB1b, MCB2b, MCB3 and MCB4 exhibited substantial axial elongation before failure.

The axial elongations of the specimens MCB1b, MCB2b, MCB3 and MCB4 varied with the loading stage as described below. At small applied load, when the beams had not cracked yet and were still elastic, there was basically no axial elongation. However, at higher applied load, when flexural and inclined shear cracks were formed, the beams started to gradually elongate in the axial direction. After the longitudinal reinforcement bars in the beam specimens had yielded, the axial elongations of the beams continued to increase at even faster rates. At the post-peak stage, despite gradual reduction in applied load, the axial elongations of the beams kept on increasing. Eventually, when the beam specimens failed, the average elongation strains of the beam specimens reached their maximum values of 2.0 to 3.5%. Such elongation strains were more than sufficient to cause all longitudinal reinforcement bars in the beams to yield. This explains why in each beam specimen, all the longitudinal reinforcement bars were in tension within the whole length of the beam before the beam failed. The beam specimens with different span/depth ratios elongated by different amounts. Basically, the smaller the span/depth ratio was, the larger was the average axial elongation strain when the beam failed.

Although axial elongation was first observed some thirty years ago (Paulay 1971), there had been little studies on the causes of axial elongation. An attempt to explain the occurrence of axial elongation is made in the following. As the shear load applied to the coupling beam increased, at a certain stage, flexural cracks appeared at the tension corners of the beam-wall joints and inclined shear cracks were formed near the center of the beam. After then, the compression diagonal of the beam acted like a diagonal concrete strut. As the two ends of the beam were subjected to further shear load (or more precisely, further shear displacement), the flexural cracks at the beam-wall joints gradually opened up and the beam as a whole started to rotate about the beam-wall joints, as shown in Fig. 8(b). The opening up of the flexural cracks at the beam-wall joints became more conspicuous after the main reinforcement bars there had yielded. This resulted in finite rotations at the beam-wall joints. At this stage, the diagonal concrete strut embedded inside the beam rotated about the compression corners of the beam-wall joints as if it was a strut member pin-jointed at the compression corners. It was the rotation of the diagonal concrete strut that caused axial elongation of the coupling beam. Applying simple kinematic calculations, the axial elongation due to rotation of the diagonal concrete strut may be estimated as (beam depth/beam span) times the lateral deflection, as depicted by dashed lines in Fig. 8(b). Because of compression shortening of the diagonal concrete strut, the actual amount of axial elongation was smaller than such an estimated value. Nevertheless, this explains the observation that the smaller the span/depth ratio of the beam was, the larger was the amount of axial elongation.

3.6 Local deformations at beam-wall joints

Previous study based on elastic analysis by the second author (Kwan 1993) had revealed that the
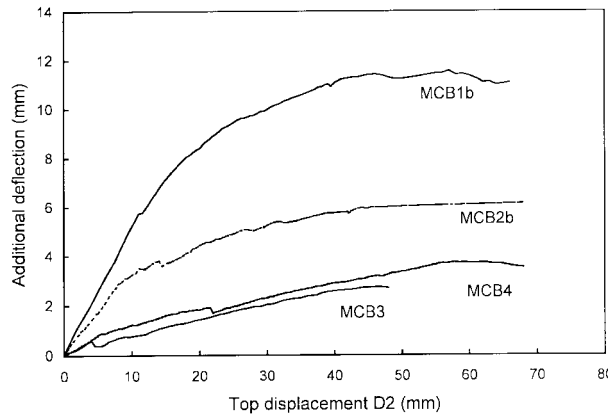
Fig. 9 Additional deflections due to lateral displacements of beam ends

local deformations of the walls at the beam-wall joints would cause lateral displacements and rotations of the beam ends relative to the walls connected to the two ends of the coupling beam. Such beam end displacements and rotations had been observed throughout the tests of the coupling beam specimens. In the following, the lateral displacements and rotations of the beam ends due to local deformations at the beam-wall joints of the specimens MCB1b, MCB2b, MCB3 and MCB4 are studied.

In Fig. 9, the additional deflections of the coupling beams arising from the lateral displacements of the beam ends due to local deformations at the beam-wall joints are plotted against the corresponding total deflections of the coupling beam specimens. It is seen that in each case, the additional deflection due to lateral displacements of the beam ends relative to the wall panels at the ends of the coupling beam gradually increased as the deflection of the coupling beam specimen increased. At the post-peak stage, the additional deflections arising from the lateral displacements of the beam ends amounted to about 25%, 10%, 6% and 6% of the corresponding total deflections for the specimens MCB1b, MCB2b, MCB3 and MCB4 respectively. In general, the smaller the span/ depth ratio of the coupling beam was, the greater was the percentage contribution of the lateral displacements of the beam ends towards the total deflection. It is believed that the apparent slightly larger additional deflection in specimen MCB4 than the additional deflection in specimen MCB3 was caused by experimental errors.

The cross-sectional rotations of the coupling beam specimens at various locations along their longitudinal axis had been measured by LVDTs during the tests to study how the sectional rotations varied along the longitudinal axis of the beam specimens. It was found that in each of the cases studied, due to the presence of flexural cracks at the beam-wall joints, the sectional rotation of the beam specimen did not vary continuously across the beam-wall joints; there were often discrete changes of sectional rotation at the beam-wall joints, especially at the post-peak stage when the cracks there opened up quite widely. As a result, there were two sectional rotations at each beam-wall joint, one at the wall side of the beam-wall joint (denoted by θ_1) and the other at the beam side of the beam-wall joint (denoted by θ_2). The sectional rotation θ_1 was caused mainly by the local deformation of the wall panel, while the difference between θ_1 and θ_2 was actually the finite rotation of the joint due to opening up of the crack and pull-out of the main reinforcement bars at the joint.

(a) Rotations of beam ends taken as the values of θ_1 (b) Rotations of beam ends taken as the values of θ_2
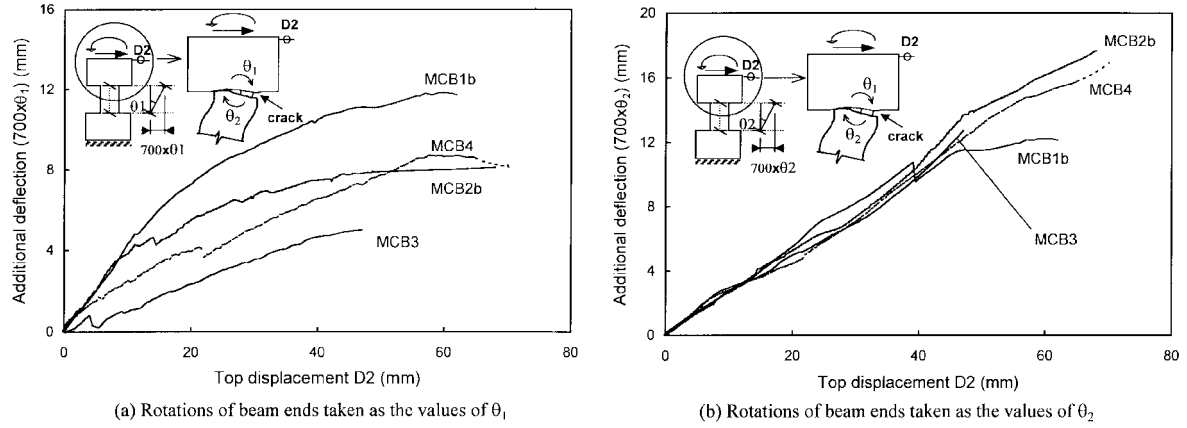
Fig. 10 Additional deflections due to rotations of beam ends

In Fig. 10(a), the additional deflections of the coupling beams arising from the rotations of the beam ends taken as the values of θ_1 at the beam-wall joints are plotted against the total deflections of the coupling beam specimens. It can be seen that at the post-peak stage, the additional deflections of the coupling beams determined in this way contributed up to about 20%, 14%, 11% and 15% of the total deflections for the specimens MCB1b, MCB2b, MCB3 and MCB4 respectively. Roughly, at a given lateral deflection, the value of θ_1 was larger in a coupling beam specimen with a smaller span/depth ratio. The larger additional deflection in MCB4 than that in MCB3 was most probably due to experimental errors. In Fig. 10(b), the additional deflections of the coupling beams arising from the rotations of the beam ends taken as the values of θ_2 at the beam-wall joints are plotted against the total deflections of the coupling beam specimens. It is evident that in each coupling beam, the additional deflection determined in this way contributed a fixed proportion of about 26% to the total deflection throughout the test regardless of the span/depth ratio of the coupling beam. This was because although θ_1 decreased with the span/depth ratio, $(\theta_1 - \theta_2)$ increased with the span/depth ratio. When added together, the value of θ_2 at a given lateral deflection appeared to be independent of the span/depth ratio of the coupling beam.

Adding the additional deflections due to lateral displacements of the beam ends and the additional deflections due to rotations of the beam ends, it can be seen that the local deformations at the beam-wall joints could contribute 30-50% to the total lateral deflection, depending on the span/depth ratio of the coupling beam.

4. Conclusions

The nonlinear behavior of deep conventionally reinforced concrete coupling beams had been investigated by testing 1/2-scale models of coupling beams using a test method that ensured equal end rotations of the beam specimen and allowed for local deformations at the beam-wall joints. From the investigation, the following conclusions regarding the characteristics of conventionally reinforced concrete coupling beams with span/depth ratios between 1.17 and 2.00 under the conditions of these tests may be drawn.

(1) After the appearance of flexural cracks at the beam-wall joints and inclined shear cracks near

the center, a deep coupling beam would behave more like a truss with the compression diagonal of the beam acting as a diagonal strut and would start to rotate about the beam-wall joints. As a result, the coupling beam would elongate in the axial direction and the longitudinal reinforcement would all become in tension within the entire span length of the beam.

(2) A coupling beam might fail either in shear or in flexure, depending on the span/depth ratio and the reinforcement details. The failure load of a deep coupling beam could be quite accurately predicted by the method given in ACI 318-95. However, the additional longitudinal reinforcement placed near mid-depth of the beam section must be taken into account because it could contribute significantly to the flexural strength of the coupling beam.

(3) Whilst a coupling beam failing in shear would have a relatively low ductility, a coupling beam failing in flexure could have a ductility ratio of 10 or higher. Hence, as far as possible, a coupling beam should be designed to fail in flexure by designing the coupling beam to have a shear strength at least 20% higher than the flexural strength.

(4) Local deformation of the walls at the beam-wall joints would cause both lateral displacements and rotations of the beam ends at the joints. Moreover, due to opening up of cracks and pull-out of the main reinforcement bars at the beam-wall joints, there could be finite rotations at the beam-wall joints. Such local deformations at the beam-wall joints could cause an additional deflection of the coupling beam amounting to 30-50% of the total deflection.

Acknowledgements

References

ACI Committee 318 (1995), *Building Code Requirements for Structural Concrete (ACI 318-95) and Commentary (ACI 318R-95)*, American Concrete Institute, U.S.A.

Aktan, A.E. and Bertero, V.V. (1984), "Seismic response of r/c frame-wall structures", *J. Struct. Eng.,* ASCE, **110**(8), 1803-1821.

Aristizabal-Ochoa, J.D. (1982), "Dynamic response of coupled wall systems", *J. Struct. Div.,* ASCE, **108**(ST8), 1846-1857.

Barney, G.B., Shiu, K.N., Rabbat, B.G., Fiorato, A.E., Russell, H.G. and Corley, W.G. (1980), "Behavior of coupling beams under load reversals", *Research and Development Bulletin RD068.01B*, Portland Cement Association, U.S.A.

Kwan, A.K.H. (1993), "Local deformations and rotational d.o.f. at beam-wall joints", *Comput. Struct.*, **48**(4), 615-625.

Kwan, A.K.H. and Zhao, Z.Z. (1998), "Nonlinear behaviour of reinforced concrete coupling beams", *Proc. ′5 Int. Conf. Tall Buildings,* Hong Kong, **1**, 410-415.

Kwan, A.K.H. and Zhao, Z.Z. (1999), "Reinforced concrete coupling beams: their differences from ordinary beams", *Proc. 7th Int. Conf. Enhancement and Promotion of Computational Methods in Engineering and Science* EPMESC VII, Macao, **1**, 581-588.

Lybas, J.M. (1981), "Concrete coupled walls: earthquake tests", *J. Struct. Div.*, ASCE, **107**(ST5), 835-855.

Paulay, T. (1970), "An elasto-plastic analysis of coupled shear walls", *ACI Struct. J.*, **67**(11), 915-922.

Paulay, T. (1971), "Coupling beams of reinforced concrete shear walls", *J. Struct. Div.*, ASCE, **97**(ST3), 843-862.

Paulay, T. and Binney, J.R. (1974), "Diagonally reinforced coupling beams of shear walls", *ACI Special Publication SP-42: Shear in Reinforced Concrete*, American Concrete Institute, Detroit, USA, **2**, 579-598.

Tassios, T.P., Moretti, M. and Bezas, A. (1996), "On the behavior and ductility of reinforced concrete coupling beams of shear walls", *ACI Struct. J.*, **93**(6), 711-720.